880034

National Research Council Canada | Conseil national de recherches Canada

Canada

Reprinted from | Réimpression du

Canadian Journal of Civil Engineering

Revue canadienne de génie civil

Thermal budget of river ice covers during breakup

T. D. Prowse and P. Marsh

Volume 16 • Number 1 • 1989

Pages 62–71

Printed in Canada / Imprimé au Canada

90-05381/

Thermal budget of river ice covers during breakup

T. D. Prowse and P. Marsh

Northern Hydrology Section, National Hydrology Research Institute, Environment Canada, Saskatoon, Sask., Canada S7N 3H5

Received January 25, 1988

Revised manuscript accepted August 29, 1988

The magnitude and relative importance of atmospheric (air–ice) and hydrothermal (water–ice) heat fluxes to intact and fragmented river ice covers are studied for the case of a thermal breakup. Based on field measurements obtained from the Liard River, the atmospheric sources are shown to be dominant during the period of intact ice cover. Radiation was the primary heat source, but its effect was reduced by a granulation of the decaying columnar ice which increased the cover albedo to that comparable for melting snow. The hydrothermal heat input, even with frazil ice entrained within the flow, was comparable to that from atmospheric sources under low melt conditions. The hydrothermal heat flux dramatically increased with the arrival of the breakup front because of a rapid rise in water temperature and an increase in subsurface ice roughness. Higher surface roughness and lower albedo of the fragmented ice also increased the atmospheric heat fluxes, but these were small relative to the hydrothermal heat input near the leading edge of open water.

Key words: floating ice, ice breakup, ice jams, ice melt.

Cet article examine l'intensité et l'importance relative des flux de chaleur atmosphérique (air–glace) et hydrothermique (eau–glace) dans les couvertures de glace de rivière intacte et fragmentée lors d'une débâcle. Des mesures effectuées sur la rivière Liard ont démontré que les sources atmosphériques étaient les plus importantes lorsque a couverture de glace est intacte. Le rayonnement a constitué la principale source de chaleur mais ses effets ont été minimisés par une granulation de la glace columnaire en désintégration qui a eu pour effet d'augmenter l'albédo de la couverture à un niveau comparable à celui de la neige fondante. L'apport de chaleur hydrothermique, même en présence de frasil entrainé par le courant, s'est avéré comparable à celui généré par des sources de chaleur atmosphérique dans des conditions de fonte lente. Le flux de chaleur hydrothermique a augmenté de façon importante avec l'arrivée du front de la débâcle en raison d'une élévation rapide de la température de l'eau et d'une augmentation de la rugosité de la glace de subsurface. Une rugosité de surface plus élevée et un albédo de la glace fragmentée plus faible ont également provoqué une augmentation des flux de chaleur atmosphérique; ces derniers étaient toutefois de faible importance si on les compare à l'apport de chaleur hydrothermique mesuré près du front d'ondes en zone d'eau libre.

Mots clés : glace flottante, débâcle, embâcles, fonte des glaces.

[Traduit par la revue]

Can. J. Civ. Eng. **16**, 62–71 (1989)

Introduction

The breakup of river ice covers is usually preceded by a decay or ablation period during which the thickness and strength of the ice sheet decrease. There are two extremes in breakup conditions: namely, "mechanical" and "thermal," with melt processes playing a large role in the latter. Mechanical breakup conditions involve a rapid increase in the stage caused by spring snowmelt and sometimes augmented by rainfall. This increased stage is often associated with a rapid moving breakup front which dislodges, fragments, and carries the ice cover downstream. The most dramatic mechanical breakups occur where upstream melt drives a breakup front into colder, downstream reaches, where much of the ice cover and surrounding land remain snow covered. In contrast, thermal breakup conditions are characterized by extensive or prolonged melt, which eliminates the snow cover and ablates the underlying ice until the cover is finally dislodged by the hydraulic forces. In some cases, the cover will melt in situ, much like what occurs on lakes.

An ice cover can melt at the surface from atmospheric heat fluxes and at the bottom from heat supplied by the flow. Ashton (1973) pointed out that significant melt of the ice bottom can occur even when the water temperature is only a few hundredths of a degree above 0°C. Green and Outcalt (1985) suggested that heat flux to the ice cover is more sensitive to variation in subsurface conditions (water temperature and velocity) than to changes in meteorological conditions. Prolonged melt periods create the best conditions for warming of the subsurface flow. Despite the apparent importance of subsurface melt, little data exist about the magnitude of hydrothermal heat fluxes or even on the water temperature beneath ice covers, especially during the breakup period. This has been due partly to logistic problems of obtaining measurements in near breakup conditions and to the difficulty in measuring water temperatures accurately within a few thousandths of a degree. Data are equally limited about the physical conditions which govern the late season melt of the ice cover surface. Wake and Rumer (1979) have noted the effect of meltwater ponds on the surface energy balance, but little else is known about conditions after the surface snow cover has melted and the meltwater drained.

Even less is known about the melt processes after breakup begins. Although melt is often cited as an important factor in ice clearance and in the release of some ice jams (e.g., Andres and Doyle 1984; Parkinson 1982; Prowse and Marsh 1985), field data concerning heat fluxes to fragmented or brash ice covers are almost nonexistent. More specifically, no measurements have been made from which the relative importance of atmospheric and hydrothermal heat fluxes to either fragmented ice covers or intact ice sheets under thermal breakup conditions can be determined.

This paper reports on a field program conducted during the late stages of a thermal breakup. Information is provided about the rise in water temperatures associated with breakup advance and changes in ice conditions which control both the surface and subsurface heat fluxes. Comparisons are made of the magnitude and relative importance of these heat fluxes to ice ablation.

NOTE: Written discussion of this paper is welcomed and will be received by the Editor until June 30, 1989 (address inside front cover).

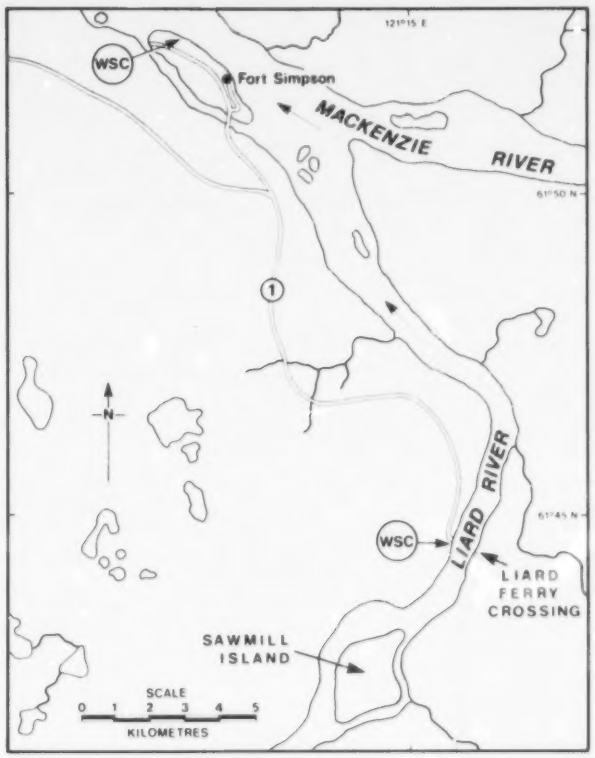

FIG. 1. The Liard River study area.

Study area

The study was carried out on the Liard River in the vicinity of its confluence with the Mackenzie River near Fort Simpson, N.W.T. (61°53′N, 121°22′W) (Fig. 1). The Liard River near its mouth drains 277 000 km^2 with a mean annual discharge of 2580 m^3/s (Environment Canada 1980*a*). Minimum mean monthly flow occurs in March, after which discharge gradually rises until May when it rapidly increases in response to snowmelt. Breakup of the Liard River near its mouth occurs in early May with the first deterioration of the snow and ice cover beginning in late April. Anderson and Fogarasi (1981) attribute the downstream progression of the Liard breakup to the gradual influx of warm Pacific air masses which replace cold Arctic air. As for most rivers, water temperature data for the Liard River during the breakup period are almost nonexistent. From post-breakup measurements, however, it is known that the river consistently warms to approximately 5°C within a few days of the removal of the ice cover and reaches a maximum water temperature of approximately 18°C in midsummer (Environment Canada 1980*b*).

The process of ice clearance usually includes the formation of an ice jam at the Liard River mouth which extends approximately 20 km upstream (Prowse 1986). Prowse and Marsh (1985) found hydrothermal melt to be an important factor in the decay of the 1983 ice jam at this site.

Field measurements for this study were conducted in the vicinity of the Water Survey of Canada gauge (noted as WSC in Fig. 1). The head of most ice jams occupies this reach, which is 700 m wide, averages 2 m in depth in late April, and has a slope of 0.00037.

Heat transfer theory

Surface energy exchanges

Atmospheric heat fluxes to a river ice sheet can be written as

$$[1] \quad Q_a = Q_* + Q_h + Q_e + Q_p$$

where Q_a is the total atmospheric heat flux, Q_* is net radiation, and Q_h, Q_e, and Q_p are the sensible, latent, and precipitation heat fluxes respectively. Positive values indicate energy gains to the ice. During this study no precipitation occurred and Q_p is therefore ignored in [1].

Radiation heat flow is the balance of short- and long-wave radiation:

$$[2] \quad Q_* = S_i(1 - \alpha)(1 - e^{-\nu t}) + L_*$$

where S_i is the global (combined direct and diffuse) solar or short-wave radiation, α is the albedo to short-wave radiation, ν is the short-wave extinction coefficient for the ice cover, t is the cover thickness, and L_* is the net long-wave radiation. In [2], $S_i(1 - \alpha)$ represents the solar radiation penetrating into the cover. Of this amount, $e^{-\nu t}$ part of it will pass out at the bottom into the water.

The fluxes of sensible and latent heat can be calculated using bulk aerodynamic formulae, which have been found by Moore (1983) to provide reliable daily or shorter term estimates of melt. The formula for sensible heat transfer can be written as

$$[3] \quad Q_h = \rho_a C_p D_h (T_a - T_i)$$

where ρ_a is the air density, C_p is the specific heat of air at constant pressure, D_h is the exchange coefficient for sensible heat, T_a is the air temperature at height z, and T_i is the snow–ice surface temperature.

Similarly, the latent heat formula can be written as

$$[4] \quad Q_e = \rho_a L_v D_e \gamma (e_a - e_i)/P$$

where L_v is the latent heat of vaporization of water, D_e is the exchange coefficient for latent heat, γ is the ratio of molecular weights of water and air, e_a and e_i are the vapour pressures above the ice at height z and at the ice surface, and P is the atmospheric pressure.

D_h and D_e are assumed equal to that of momentum (D_m), so that under neutral conditions,

$$[5] \quad D_h = D_e = D_m = \frac{k^2 u}{[\ln(z/z_0)]^2}$$

where k is von Karman's constant, equal to 0.4; u is the wind velocity at height z; and z_0 is the roughness length. To account for nonneutral conditions, [5] must be multiplied by a stability factor (β) which is set to (Price and Dunne 1976)

$$[6] \quad \beta = 1/(1 + \sigma Ri)$$

for stable conditions, and

$$[7] \quad \beta = 1 - \sigma Ri$$

for unstable conditions, where σ is a constant approximately equal to 10 (Webb 1970) and Ri is a bulk form of the Richardson number defined as

$$[8] \quad Ri = \frac{gz\Delta T_a}{T_a(\Delta u)^2}$$

where g is the acceleration due to gravity, ΔT_a and Δu are the air temperature (°K) and wind speed differences between the surface and height z.

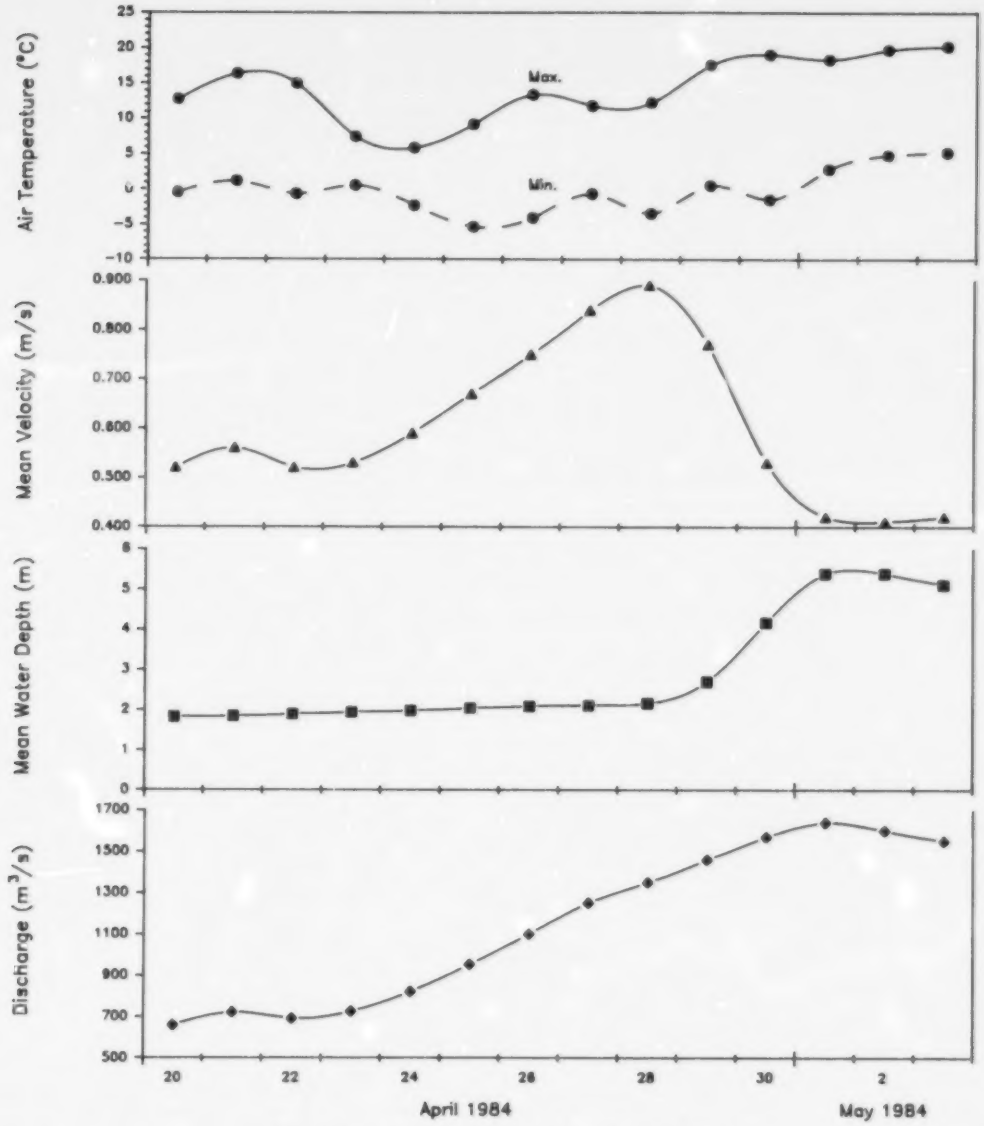

FIG. 2. Prevailing hydrometeorological conditions.

Subsurface energy exchange

Under ice-covered conditions, the major heat fluxes to the flow can be written as

$$[9] \quad Q_\Sigma = Q_s + Q_L + Q_g + Q_b + Q_c + Q_f$$

where Q_Σ is the combined sources of local heat, Q_S and Q_L are the short-wave and long-wave radiation fluxes absorbed by the flow, Q_g is the heat flux from groundwater flow, Q_b is the bed heat flux resulting from geothermal flux and the release of sensible heat stored during the previous open water period, Q_c is the heat flux from local surface runoff and tributary streams, and Q_f is the heat flux due to fluid friction. Positive values indicate energy gains to the flow. The magnitude and relative importance of these terms vary according to both hydraulic and meteorological conditions. The greatest variability, however, occurs in Q_S on a daily basis because of diurnal fluctuations in S_i, and over the pre-breakup period because of the decrease in albedo and radiation attentuation within the cover as the snow and snow-ice layers are albated. Considering both gains and losses, the heat budget of the flow can be written as (adapted from Wankiewicz (1984))

$$[10] \quad -C_v DV\frac{dT_w}{dx} - Q_i - Q_w + Q_\Sigma = 0$$

where the first term is the rate of heat supplied by convection of flowing water with heat capacity per unit volume, C_v; D is flow depth; V is average flow velocity; and dT_w/dx is the downstream temperature gradient in which T_w is the bulk water temperature at a distance x from the section entrance. Q_i is the heat flux to ice entrained within the flow and Q_w is the heat flux from the flow to the bottom of the ice cover.

The physical process of convective heat transport from the water to the ice bottom is similar to the heat transfer at an air–ice boundary. The heat transfer equation, therefore, should be similar to [3] and is written here in the form of

$$[11] \quad Q_w = \phi_w(T_w - T_s)$$

where T_s is the ice temperature at the water–ice interface and ϕ_w is the heat transfer coefficient which lumps the equivalent of the three parameters in [3] together. In a review and testing of water–ice heat transfer theories, Marsh and Prowse (1987) found that ϕ_w can be best described by

$$[12] \quad \phi_w = C_v V S_t$$

where S_t is the Stanton number for heat transfer defined as

$$[13] \quad S_t = \frac{g n_i^2 [1 + (n_b/n_i)^{3/2}]^{1/3}}{K_m^2 P_r^{2/3} D^{1/3}}$$

where n_b and n_i are the Manning bed and ice roughness respectively, K_m is a Manning unit conversion factor, and P_r is the Prandtl number for water. Despite the outward difference of the expressions of $\phi_w = C_v V S_t$ and $\rho_a C_p D_h$, they describe the same turbulent heat transfer process. The appearance of n_b and D in the former really means that the turbulent heat transfer process at the ice–water boundary is affected by the velocity distribution, which is determined by, besides the ice cover bottom roughness, the river bed roughness and the depth of flow.

Field measurements and calculations

Hydrometeorological conditions

The field study was conducted in the spring of 1984. The hydrometeorological conditions prevailing over the breakup period are shown in Fig. 2. Although snow depths were slightly above normal at the beginning of April, warm conditions rapidly depleted the snowpack to below normal levels within several days and to only a trace by April 20—more than 20 days earlier than the long-term mean date (Atmospheric Environment Service, unpublished). At the same time, flow on the Liard River was 36% above normal at 658 m^3/s.

Data collection began once most of the surface snow cover had melted and drained from the surface. Unfortunately, because of rapidly deteriorating conditions, instruments for measuring the surface energy balance had to be removed after only a few days of recording. Fortunately, however, the sample period was representative of high melt conditions. Breakup occurred on April 29 with the arrival of a breakup front at the gauging station at 18:00 Mountain Standard Time. An ice jam developed at the Liard River mouth later that evening forming a brash ice accumulation which extended several kilometres upstream of the study site. Final release of this jam into the Mackenzie River occurred on May 4. More detailed discussion of the hydraulic and hydrometeorological conditions can be found in Prowse (1985, 1986).

Intact ice cover

Instrumentation used to measure the surface energy balance is shown in Fig. 3. Meteorological data were recorded at a sampling frequency of once every 10 s. Air temperature and relative humidity was measured using aspirated thermistors and sulfonated polystyrene humidity sensors. Total maximum system error for the temperature measurements from −20 to 35°C was ±0.4°C. Relative humidity sensor output was linear to ±3% from 10 to 97%. Vapour pressures were obtained by the Goff-Gratch and Teton formulations as reviewed by Sargent (1980, 1982). Micro-response contact anemometers with a threshold speed of 0.32 m/s were used to measure wind speed.

Net radiation was measured with a net pyrradiometer (0.3–60 μm) and incoming and outgoing short-wave radiation were measured with a two-component pyranometer. A weighted extinction coefficient was used in [2] based on measured

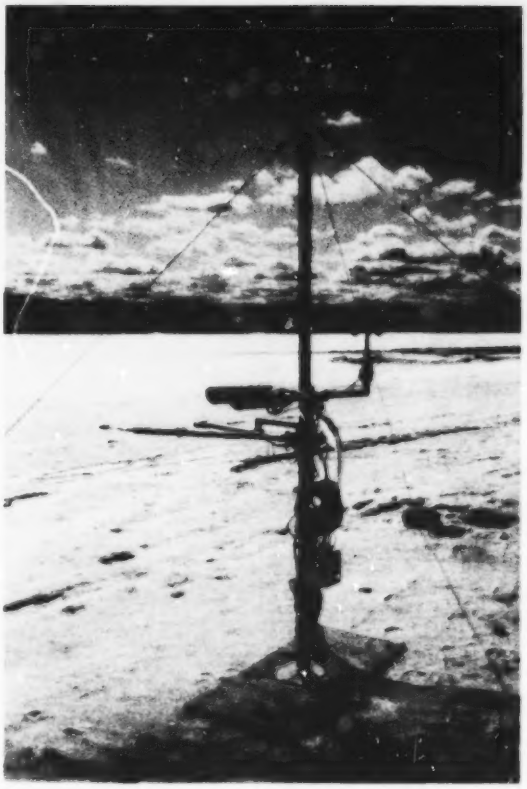

FIG. 3. Instrumentation for measuring surface energy balance.

thicknesses of principal ice strata and corresponding values of γ obtained from the literature (Prowse and Stephenson 1986). The mean thicknesses of the principal ice layers, obtained from a 20-point cross-section survey conducted on April 25, were 0.10 m of surface white ice, 0.86 m of black ice, and 0.24 m of underlying, dense slush ice. ν was set to 2.0 for black ice and 4.0 for white and slush ice. Net long-wave radiation was computed as the residual term in [2]. The value of z_0 for the intact cover was obtained from wind measurements at two heights (z_1 and z_2) under neutral conditions according to

$$[14] \quad z_0 = \exp \frac{(u_2 \ln z_1 - u_1 \ln z_2)}{(u_2 - u_1)}$$

The resultant mean value of 2.14×10^{-3} m is similar to the value of 2.5×10^{-3} m originally proposed by Sverdrup (1936) and commonly used in energy balance studies of relatively smooth snow and ice surfaces.

Water temperature measurements were made using thermistors calibrated in a temperature bath using a standard platinum resistance thermometer originally calibrated by the National Research Council of Canada at fixed points on the international temperature scale (Judge 1973). The platinum resistance thermometer was checked occasionally in a triple-point cell (Judge 1973) and is acurate to ±0.002°C relative to the National Research Council of Canada standards. Normally the absolute accuracy of temperature measurements is limited to ±0.01°C because of the uncertainty involved in defining fixed points on the international practical temperature scale of 1968 (IPTS-68 1969). However, since measurements for the present study were made over a narrow range of temperatures which were within ±0.01°C of the triple point of water, which is a fixed, exactly

defined point on the international practical temperature scale (IPTS-68 1969), the accuracy of the calibration of these thermistors is believed to be better than ±0.005°C. In the field, resistances were measured with a DC Wheatstone resistance bridge especially designed for accurate field measurements of temperature (Judge 1973).

Vertical profiles of flow velocity and water temperature were measured daily at 30 m intervals across the channel beneath the intact ice over. After the intact ice cover became unsafe for travel, single point measurements of water temperature were obtained daily from thermistor cables located 200 and 300 m from shore. Values of n_b and n_i were calculated using the regression method outlined by Pratte (1979). Although an increase in n_i was expected as melt progressed and ice ripples were observed on the bottom of the ice cover (Marsh and Prowse 1987), no temporal trend was observed in the data. This could have been due to the velocity profile method being not sufficiently sensitive to detect changes in the ice-bottom roughness that might have occurred over the study period. As a result, mean values of $n_i = 0.025$ and $n_b = 0.031$ were used. Mean daily discharge of the Mackenzie and Liard rivers was obtained from Water Survey of Canada.

Fragmented ice cover

Logistic difficulties created by an unstable ice surface precluded the direct measurement of the energy balance over the brash ice surface. Instead, the atmospheric heat fluxes were modelled based on the same meteorological conditions which were measured over the intact ice sheet. The simulation also required values for the albedo and higher surface roughness of the brash ice surface.

A separate experiment (Prowse 1987) was conducted to obtain a representative albedo. During the 1985 breakup, conditions created by a slow releasing ice jam allowed the measurement of the spatially averaged, brash ice albedo by extending an albedometer over the moving, congested ice. Table 1 gives the prevailing sky conditions and measured range in albedo values for global solar radiation. The average value of $\alpha = 0.08$ was used in the energy balance simulation.

The surface roughness of the brash ice accumulations was estimated using the approach outlined by Lettau (1969) in which z_0 is estimated from the height and basal and silhouette area of surface forms:

$$[15] \quad z_0 = hS/2B$$

where h is the obstacle height, S is the silhouette area in the downwind plane, and B is the basal area of the obstacle. Using field observations of form shape and size of brash ice surfaces gave $z_0 = 0.07$ m.

After ice movement began and an ice jam developed, water temperatures and velocity were measured from a helicopter at the upstream edge of the ice jam and in holes within the jam using an electromagnetic velocity meter. From knowledge of n_b measured during the period of intact cover, flow depth, and the point of maximum velocity, the method of Komora and Sumbal (1967) was used to derive the bottom roughness of the ice jam cover, $n_i = 0.055$.

For both the case of intact and fragmented ice, an estimate of the potential thinning of the cover produced by the heat fluxes at the atmosphere–ice and water–ice interfaces was calculated on a daily basis using

$$[16] \quad M_i = Q/\rho_i L_i$$

where M_i is the daily melt of ice, Q is the total daily heat flux at the relevant interface, ρ_i is the density of ice (assumed to be 920 kg/m^3), and L_i is the latent heat of fusion for ice. In the case of surface melt, a portion of M_i is distributed through the ice sheet because of the penetration of solar radiation.

TABLE 1. Albedo of brash and decaying black ice. (All measurements were conducted under clear sky conditions.)

Ice type	Albedo	Solar altitude (Degree)
Brash: mean	0.08	
max.	0.15	30–38
min.	0.04	
Crystal pavement	0.17	43
Candled black ice	0.39	41
Granulated black ice	0.55	42

Results and discussion

Intact ice cover—atmospheric heat flux

Results of the surface energy balance conducted over the period April 22–25 are shown in Fig. 4. Because most heat fluxes exhibit diurnal fluctuations, daily heat flux sums are presented for comparison purposes in Table 2. Also listed are the associated meteorological parameters. Note, however, that the daily heat flux sums were derived from hourly averages and were not calculated from the daily averages of meteorological conditions listed at the top of Table 2.

The total atmospheric heat flux to the intact ice cover ranged from 1.73 to 5.70 MJ·m^{-2}·d^{-1}. Using [16], this translates into a melt of 5.6–18.6 mm/d of ice. In general, surface meteorological conditions were representative of high radiation melt in which Q_* ranged from 2.90 to 5.27 MJ·m^{-2}·d^{-1} and accounted for 65–100% of the daily positive heat flow. Net radiation would have been even greater if not for the large values of α (Table 2) which significantly reduced the net effect of solar radiation. Although this study was conducted after most of the surface snow and snow-ice had melted and exposed the underlying columnar black ice, the surface had an unexpectedly high albedo.

Popular belief is that black ice has the lowest albedo of the various snow and ice types. Bolsenga (1969), for example, reports a value of 0.1 for clear, snow-free lake ice, comparable to that of open water. During the period of energy balance monitoring, however, the mean daily albedo of the black ice surface actually increased from 0.40 to 0.52, a value similar to that for well-ripened snow (Table 2). This dichotomy can be explained by an acicular melting of the black ice which eventually leads to a granulation of the crystal tops. Figure 5*a–d* shows the progressive stages of this process documented as part of a larger study of radiation-melt processes. The corresponding albedo values are listed in Table 1. Initially, the surface was etched as the individual crystal perimeters began to preferentially melt; the first stage in the candling process. As this process continued, the tops of the crystals granulated and separated from the underlying black ice, giving the surface an appearance similar to that of melting snow or snow-ice (Fig. 5*d*). Hence, only during the very early stages of decay is black ice characterized by a very low albedo. In the later stages of melt, such as experienced between April 22 and April 25, granulation of the top crystals actually serves to insulate the underlying ice from solar radiation.

Relative to the radiative terms, inputs of sensible and latent heat were from moderate to slightly negative (i.e., −1.07 to

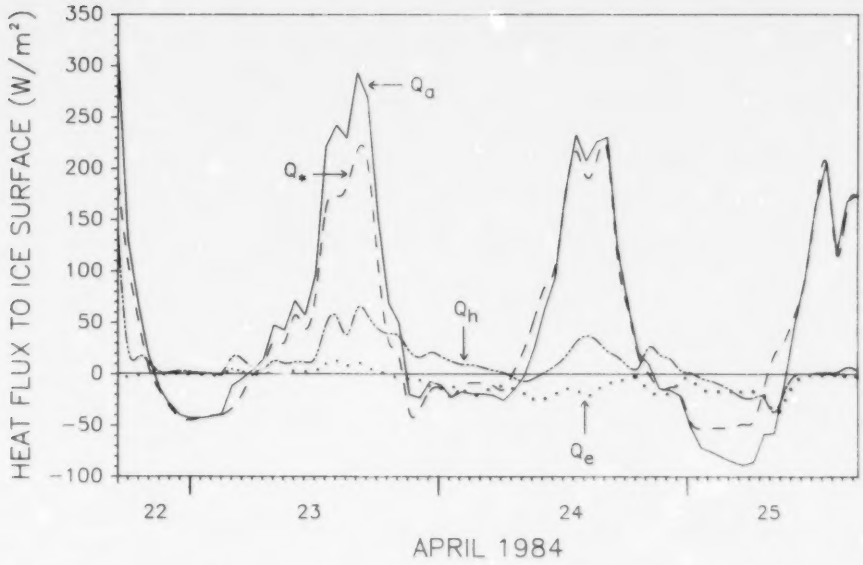

FIG. 4. Components of the surface heat energy balance: Q_a = total atmospheric heat flux; Q_* = net radiation; Q_h = sensible heat flux; Q_e = latent heat flux.

TABLE 2. Prevailing meteorological conditions and major heat fluxes to intact and fragmented ice

Parameter	Dates data collected		
	April 22–23	April 23–24	April 24–25
T_a mean (°C)	3.90	2.20	0.75
T_a max. (°C)	12.53	7.31	5.83
T_a min. (°C)	−1.25	−1.45	−5.36
u (m/s)	1.54	2.12	0.81
e (kPa)	0.62	0.51	0.44
S_i (MJ·m^{-2}·d^{-1})	10.53	16.51	14.99
α	0.40	0.46	0.52
Heat fluxes to intact ice (MJ·m^{-2}·d^{-1})			
Q_a	5.70	5.74	1.73
Q_*	3.69	5.27	2.90
Q_h	1.84	1.55	−0.20
Q_e	0.17	−1.07	−0.98
Q_w	1.58	1.50	2.25
(Q_w mean for the period April 20–28 = 1.78)			
Heat fluxes to fragmented ice (MJ·m^{-2}·d^{-1})			
Q_a	15.34	12.15	2.26
Q_*	6.03	9.93	7.71
Q_h	8.50	7.18	−0.91
Q_e	0.81	−4.96	−4.55
(Q_w on May 3 over the upper 4 km reach = 348.36)			

1.84 MJ·m^{-2}·d^{-1}). Greater convective heat transfer would have required higher surface roughness or steeper temperature and wind gradients. A rough surface, however, would be difficult to find because even the large surface irregularities of a freeze-up ice jam would be smoothed out after prolonged melt and refreezing.

To permit comparison of the relative importance of the various heat fluxes in subsequent sections, it is useful here to estimate the total heat flux for a case of extreme surface melt. Although theoretical maxima can be calculated for a variety of extreme meteorologic conditions, it is easier to obtain the relevant information from the literature dealing with intense snowmelt. Typical conditions for such an event involve large inputs of solar radiation and rapid transfer of sensible heat due to warm air advection. In general, the clear sky conditions which result in high values of S_i do not favour high positive values of Q_e or Q_p, and these are therefore not considered in this example. First, in terms of Q_h for intense snowmelt occurring under warm air advection, values in the range of 5 to 10 MJ·m^{-2}·d^{-1} are not uncommon (e.g., see Golding 1978; Prowse and Owens 1982). Second, considering that this study was already characterized by clear sky conditions, inputs of solar radiation to the ice cover could only be significantly increased at this time of year if a lower albedo had prevailed. For example, if the extremely low value of $\alpha = 0.1$ suggested by Bolsenga (1969) is used in [2] with measured values for S_i and the entire cover is assumed to be black ice, the total atmospheric heat values in Table 2 increase significantly to 8.33, 10.87, and 6.95 MJ·m^{-2}·d^{-1} respectively. These values combined with those for extreme Q_h indicate that Q_a for an extreme melt situation could be in the order of 20 MJ·m^{-2}·d^{-1} or almost four times that measured during this tudy.

Intact ice cover—hydrothermal heat flux

Figure 6 shows the change in water temperature and corresponding heat flux which occurred at the Liard River study site over the period April 20 to May 4, 1984. During the period of intact cover from April 20 to April 29, water temperature ranged from 0.003 to 0.010°C which, using measured values for D, V, and the fore-mentioned values for n_i and n_b in [9], [10], and [11], gives a range in heat flux of 10.4 to 29.7 W/m^2 (average of 20.6 W/m^2) (Fig. 6). Assuming these values are representative of the daily means, the corresponding daily heat inputs ranged from 1.50 to 2.25 MJ·m^{-2}·d^{-1} (over the 3-day detailed study period; Table 2) which translate into ice melt of 4.9–7.3 mm/d. On average these Q values equal 40% of that due to the atmospheric heat flows over the same period and on a daily basis approximate the Q_a value for April 24–25. They also

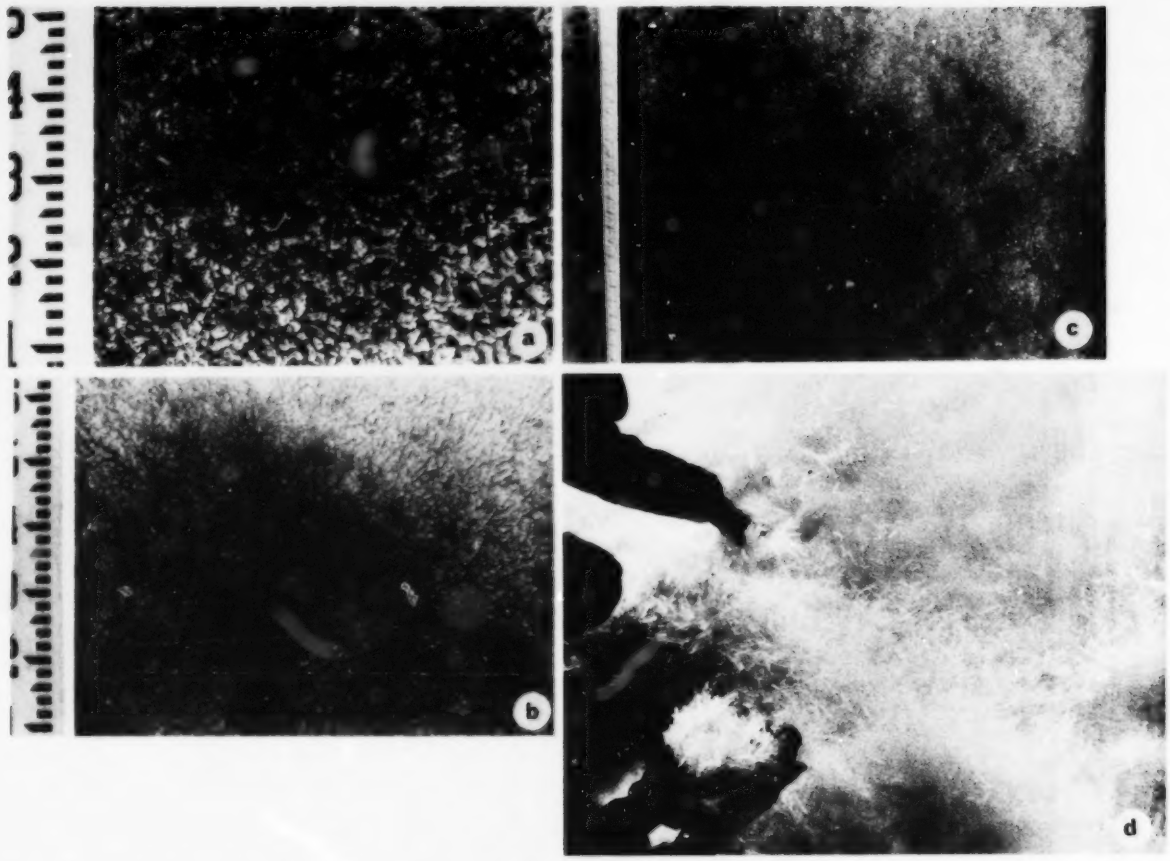

FIG. 5. Progressive decay of black ice surface: (*a*) crystal pavement, (*b*) surface candling, (*c*) granulation of crystal tops, and (*d*) decaying black ice with appearance of melting snow-ice surface. Vertical height of grid marks is approximately 3 mm. Corresponding albedo values are listed in Table 1.

equal approximately 10% of the Q_a value estimated for the extreme case of surface melt. Notably, however, much of the increase in Q_a for the extreme melt event was a result of greater net solar radiation. As shown in [2] and [9], a portion of the radiation also penetrates the cover and heats the underlying flow. For the case of $\alpha = 0.1$ discussed above (assuming a complete black ice layer with $\nu = 2.0$), inputs of solar radiation to the flow would increase by 0.53–0.88 $MJ \cdot m^{-2} \cdot d^{-1}$ or approximately double. These increases also represent a significant portion of the Q_w values in Table 2 and thereby serve to illustrate how important solar heating of the flow can be to the hydrothermal heat flux.

Although warm water temperatures might generally be expected to prevail during the latter stages of decay, particularly when solar heating of the flow is large, temperature of the flow beneath the intact cover in this study never rose above 0.01°C. During a number of discharge measurements, frazil was noted to be entrained within the flow at a number of locations across the cross section, much of it probably originating from upstream, localized deposits. As per [10], the latent heat consumed in melting this frazil (i.e., Q_i) is at least partly responsible for the relatively low water temperatures.

In view of the near 0°C water temperatures, the relatively large contribution of Q_w to total melt might seem surprising, but, as noted earlier, the heat transfer coefficient is also a function of n_b, n_i, D, and V. Although the roughness terms were assumed constant at mean measured values, both the flow depth and velocity significantly increased over the April 20–29 period (Fig. 2). Only the latter term, however, was responsible for the rise in Q_w, since ϕ_w varies inversely with flow depth. Changes in the heat transfer are also much more sensitive to changes in velocity than depth since it is only the cube root of D that appears in [13].

Fragmented ice cover—atmospheric heat flux

Results of the modelled energy balance for the brash ice surface are summarized in Table 2. Q_a, which ranged from 2.26 to 15.34 $MJ \cdot m^{-2} \cdot d^{-1}$ (ice melt of 7.4–50.0 mm/d), was 126% greater overall than that for the intact ice cover under the same atmospheric conditions. Much of this increase was due to the lower albedo for brash ice which resulted in an average 100% increase in net radiation for the 3-day period. More important, however, was the higher surface roughness which increased the flows of sensible and latent heat by 363%. Notably, this resulted in the sensible heat flow being larger than even net radiation for the first study day.

Fragmented ice cover—hydrothermal heat flux

With the advance of the break-up front into the study reach, rapid increases in water temperature were measured at the gauging station from May 1 to May 4 as shown in Fig. 6. At this site, water temperatures measured beneath the brash ice were approximately 0.04°C on May 1 and 2 but rapidly increased to

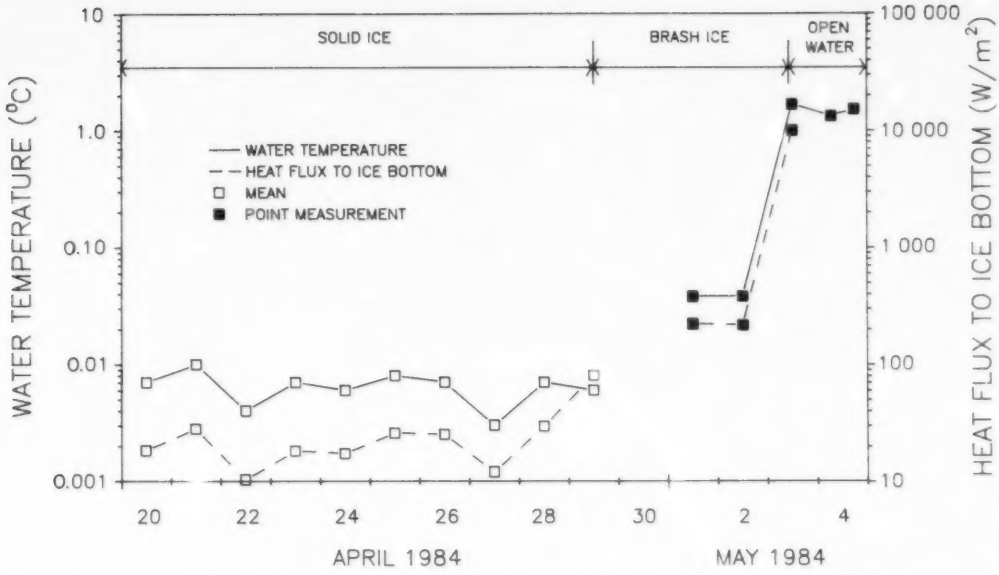

FIG. 6. Water temperature and corresponding heat flux to the base of the ice cover.

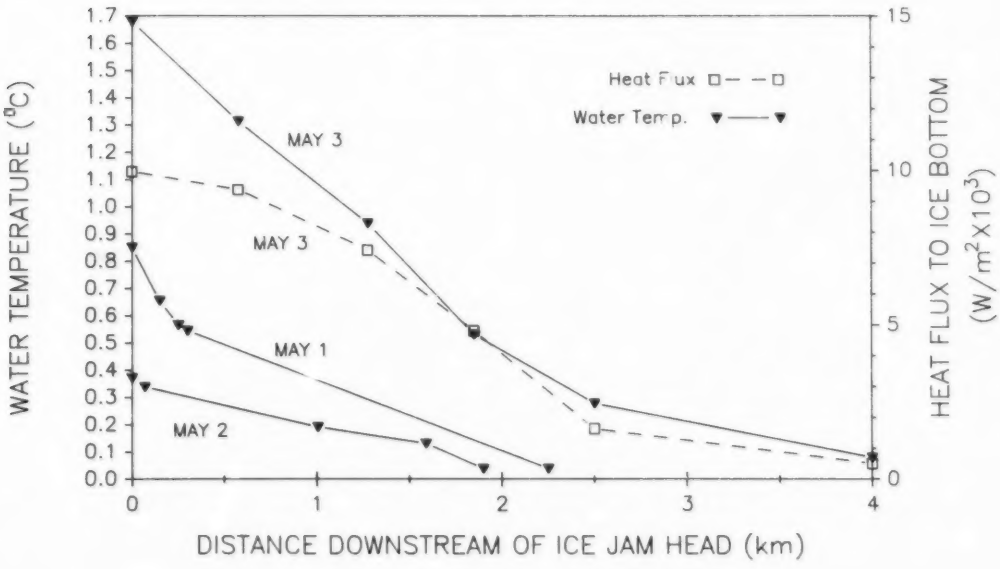

FIG. 7. Water temperature profiles and heat flux beneath brash ice.

1.68°C on May 3 with the arrival of the leading edge of open water. In terms of the parameters governing the heat flux to the ice bottom, depth increased to approximately 5 m on May 1 and remained relatively constant, velocity decreased dramatically (Fig. 2) and ice roughness increased from a pre-breakup value of 0.025–0.055. As a result of these changes, Q_w increased from a pre-breakup value of 20.6 W/m^2 to almost 10 000 W/m^2 on May 3. This latter value, however, was only representative of heat flux near the upstream end of the jam (Fig. 6) and significant variation occurred in Q_w along the length of the brash ice accumulation, primarily because of a downstream decrease in water temperature.

Measurements conducted along the jam on May 1–3 (Fig. 7) showed the water temperature to decrease rapidly from a maximum at the leading edge to near 0°C several kilometres within the ice accumulation. Heat flux to the base of the ice followed a similar decrease. On May 3, for example, Q_w decreased from approximately 10 000 W/m^2 near the leading edge of open water to only 500 W/m^2 4 km downstream (Fig. 7). Assuming constant flow and water temperature for May 3, the total daily heat input over this 4 km reach averaged 348.36 MJ·m^{-2}·d^{-1}, which translates into an ice thinning of 1.13 m/d.

In view of the exceptionally high inputs of Q_w, the total atmospheric heat flux to the brash ice appears almost insignificant even though it is an average 126% greater than that supplied to the intact ice. For example, the highest value of Q_a = 15.34 MJ·m^{-2}·d^{-1} to the fragmented cover is only 4% of the

average hydrothermal flow occurring in the upper 4 km of the ice jam. Although it could be argued, as for the case of intact ice, that Q_a could have been higher under more extreme meteorological conditions, the relative importance of Q_a to Q_w would be unlikely to drastically change. This is simply because greater atmospheric heat inputs would also result in higher upstream water temperatures being generated in upstream open-water reaches and, hence, greater Q_w. In general, the highest upstream water temperatures should result from mechanical breakups in which the ice cover is completely cleared, leaving extensive open water zones in which uninterrupted heating of the flow may occur. Lower upstream temperatures are most likely to result from thermal breakups in which the flow is alternately cooled and warmed as it passes through sequences of ice-covered and open water reaches produced by the non-sequential clearance of ice typical of thermal breakups.

Conclusions

1. Under high-melt conditions associated with a thermal breakup, atmospheric heat fluxes have been shown to dominate the decay of the intact ice cover. Radiation was the primary heat source, but its effect was reduced by a granulation of the decaying columnar ice which increased the cover albedo to that comparable for melting snow.

2. Even though water temperatures were very close to 0°C, partly because of the damping effect of frazil melted within the flow, the hydrothermal heat flux to the base of the intact cover was approximately equal to 40% of the atmospheric heat flux over the same period.

3. The hydrothermal heat flux dramatically increased with the arrival of the breakup front because of a rapid rise in temperature and an increase in subsurface ice roughness. Even once an ice jam developed, and although flow conditions (large depth and slow water velocity) did not favour a rapid heat transfer, the hydrothermal heat flux to brash ice remained high because of large subsurface roughness and high upstream water temperatures. Although this study focussed on a thermal breakup, even higher flow temperatures should be produced by mechanical breakups which progress by a sequential, downstream clearance of ice and leave long open water reaches in which uninterrupted heating of the flow can occur.

4. Large surface roughness and low albedo of the fragmented ice also increased the atmospheric heat fluxes, but these were small relative to the hydrothermal heat input in the upstream portions of the ice jam. Hence, under most conditions, the thermal decay of ice jams is primarily due to hydrothermal rather than atmospheric heat fluxes.

Acknowledgements

Thanks are due to Messrs E. Burgess, R. O. Christie, and T. Maxin for assistance with field work and the development of instrumentation; Mr. P. Wood and staff (Water Survey of Canada, Environment Canada, Fort Simpson) for logistical help in the field; Indian and Northern Affairs Canada for additional financial support and accommodation in Fort Simpson; Mr. V. Allen, Dr. A. Tylor, and Dr. A. Judge (Earth Physics Branch, Energy Mines and Resources Canada) for the loan of equipment and calibration of thermistors; and Mr. C. Bill (National Water Research Institute, Environment Canada) for the calibration and loan of current meters.

ANDERSON, J. C., and FOGARASI, S. 1981. The hydroclimatic setting of the Liard River basin spring flood. *In* Spring break-up, Mackenzie River basin study report, Supplement 3. Mackenzie River Basin Committee (Canada).

ANDRES, D. D., and DOYLE, P. F. 1984. Analysis of break-up and ice jams on the Athabasca River at Fort McMurray, Alberta. Canadian Journal of Civil Engineering, **11**: 444–458.

ASHTON, G. D. 1973. Heat transfer to river ice covers. Proceedings of the 30th Eastern Snow Conference, Amherst, MA, pp. 125–135.

BOLSENGA, S. J. 1969. Total albedo of Great Lakes ice. Water Resources Research, **5**: 1132–1133.

ENVIRONMENT CANADA. 1980*a*. Historical streamflow summary, Yukon and Northwest Territories. Water Survey of Canada.

——— 1980*b*. Sediment data, Canadian rivers. Water Survey of Canada.

GOLDING, D. L. 1978. Calculated snowpack evaporation during Chinooks along the eastern slopes of the Rocky Mountains in Alberta. Journal of Applied Meteorology, **17**: 1647–1651.

GREEN, G. M., and OUTCALT, S. I. 1985. A simulation model of river ice cover thermodynamics. Cold Regions Science and Technology, **10**: 251–262.

IPTS-68. 1969. The international practical temperature scale of 1968. Metrologia, **5**: 35–44.

JUDGE, A. S. 1973. The thermal regime of the Mackenzie Valley: Observations of the natural state. Environmental-Social Committee, Northern Pipelines, Task Force on Northern Oil Development, Report No. 73–38.

KOMARA, J., and SUMBAL, J. 1967. Head losses in channels with ice cover. Proceedings of the 12th Congress of the International Association for Hydraulic Research, No. 4, pp. 270–274.

LETTAU, H. 1969. Note on roughness-parameter estimates on the basis of roughness-element description. Journal of Applied Meteorology, **18**: 828–832.

MARSH, P., and PROWSE, T. D. 1987. Water temperature and heat flux to the base of river ice covers. Cold Regions Science and Technology, **14**: 33–50.

MOORE, R. D. 1983. On the use of bulk aerodynamic formulae over melting snow. Nordic Hydrology, **14**: 193–206.

PARKINSON, F. E. 1982. Water temperature observations during break-up on the Liard–Mackenzie river system. Proceedings of the Workshop on Hydraulics of Ice Covered Rivers, Edmonton, Alta., pp. 261–295.

PRATTE, B. D. 1979. Review of flow resistance of consolidated smooth and rough ice covers. Canadian Hydrology Symposium, 1979, Vancouver, B.C., pp. 52–92.

PRICE, A. G., and DUNNE, T. 1976. Energy balance computations of snowmelt in a subarctic area. Water Resources Research, **12**: 686–694.

PROWSE, T. D. 1985. Hydrometeorologic conditions prevailing during the 1984 river ice break-up, Fort Simpson region, N.W.T. National Hydrology Research Institute, Environment Canada, Report for the Water Resources Division, Department of Indian Affairs and Northern Development, Ottawa, Ont.

——— 1986. Ice jam characteristics, Liard–Mackenzie River confluence, N.W.T. Canadian Journal of Civil Engineering, **13**: 653–656.

——— 1987. Albedo of break-up ice covers. Proceedings of the 44th Eastern Snow Conference, Fredericton, N.B., pp. 197–202.

PROWSE, T. D., and MARSH, P. 1985. Hydrothermal decay of ice jams. Proceedings of the 42nd Eastern Snow Conference, Montréal, Que., pp. 272–276.

PROWSE, T. D., and OWENS, I. F. 1982. Energy balance over melting snow, Craigieburn Range, New Zealand. Journal of Hydrology (N.Z.), **21**: 133–147.

PROWSE, T. D., and STEPHENSON, R. L. 1986. The relationship between winter lake cover, radiation receipts and the oxygen deficits in temperate lakes. Atmosphere-Ocean, **24**: 386–403.

SARGENT, G. P. 1980. Computation of vapour pressure, dew-point and

relative humidity for dry- and wet-bulb temperatures. Meteorological Magazine, **109**: 238–246.

——— 1982. Correspondence: Comment on computation of vapour pressure, dew-point, and relative humidity from dry and wet-bulb temperatures. Meteorological Magazine, **111**: 159–160.

SVERDRUP, H. U. 1936. The eddy conductivity of the air over a smooth snow field. Geofysiske Publikasjoner, **11**: 1–69.

WAKE, A., and RUMER, R. R., JR. 1979. Effect of surface melt water accumulation on the dissipation of lake ice. Water Resources Research, **15**: 430–434.

WANKIEWICZ, A. 1984. Analysis of winter heat flow in an ice-covered Arctic stream. Canadian Journal of Civil Engineering, **11**: 430–443.

WEBB, E. K. 1970. Profile relationships: the log-linear range of extension to strong stability. Quarterly Journal of the Royal Meteorological Society, **96**: 67–90.

List of symbols

B	basal area of roughness element (m^2)
C_p	specific heat of air at constant pressure ($J \cdot kg^{-1} \cdot °C^{-1}$)
C_v	specific heat of water by volume ($J \cdot m^{-3} \cdot °C^{-1}$)
D	flow depth (m)
D_e	exchange coefficient for latent heat (m/s)
D_h	exchange coefficient for sensible heat (m/s)
D_m	exchange coefficient for momentum (m/s)
e_a	vapor pressure of air (Pa)
e_i	vapor pressure over ice (Pa)
g	acceleration of gravity (m/s^2)
h	height of roughness element (m)
K_m	Manning unit conversion factor ($m^{1/3}/s$)
k	von Karman's constant
L_i	latent heat of fusion of ice (J/kg)
L_v	latent heat of vaporization of water (J/kg)
L_*	net long-wave radiation (W/m^2)
M_i	ice melt (m/d)
n_b	Manning bed roughness
n_i	Manning ice bottom roughness
P	atmospheric pressure (Pa)
P_r	Prandtl number for water
Q	daily total of heat fluxes ($J \cdot m^{-2} \cdot d^{-1}$)
Q_a	net atmospheric heat flux (W/m^2)
Q_b	bed heat flux (W/m^2)
Q_c	heat flux from contributing flow (W/m^2)
Q_e	latent heat flux (W/m^2)
Q_f	heat flux due to flow friction (W/m^2)
Q_g	groundwater heat flux (W/m^2)
Q_h	sensible heat flux (W/m^2)
Q_i	heat flux to frazil and anchor ice (W/m^2)
Q_L	long-wave radiation absorbed by the flow (W/m^2)
Q_p	precipitation heat flux (W/m^2)
Q_S	short-wave radiation absorbed by the flow (W/m^2)
Q_w	water to ice bottom heat flux (W/m^2)
Q_Σ	net heat fluxes to river flow (W/m^2)
Q_*	net radiative heat flux to the ice surface (W/m^2)
R_i	bulk Richardson number
S	silhouette area of roughness element (m^2)
S_i	global solar radiation (W/m^2)
S_t	Stanton number for heat transfer
T_a	air temperature (°C; °K)
T_i	snow–ice surface temperature (°C)
T_s	ice–water interface temperature (°C)
T_w	water temperature (°C)
t	ice thickness (m)
u	wind velocity (m/s)
V	flow velocity (m/s)
x	downstream distance (m)
z	height (m)
z_0	roughness height (m)
α	albedo to short-wave radiation
β	stability factory
γ	ratio of molecular weights of water and air
ν	extinction coefficient (m^{-1})
ρ_a	air density (kg/m^3)
ρ_i	ice density (kg/m^3)
σ	constant for stability calculations ([6] and [7])
ϕ_w	water to ice heat transfer coefficient ($W \cdot m^{-2} \cdot °C^{-1}$)